Available online at www.eccomasproceedia.org
Eccomas Proceedia COMPDYN (2023) 4825-4838

ECCOMAS
Proceedia

COMPDYN 2023
9th ECCOMAS Thematic Conference on
Computational Methods in Structural Dynamics and Earthquake Engineering
M. Papadrakakis, M. Fragiadakis (eds.)
Athens, Greece, 12-14 June 2023

DEVELOPMENT OF A COMPLIANT MECHANISM TO ISOLATE THE BASE VIBRATIONS AND MINIMIZE THE SHOCK RESPONSE USING AN OPTIMIZED DYNAMIC MATHEMATICAL MODEL

Kazım Yüksel[1,2], **Ata Muğan**[2]

[1] ASELSAN A.Ş.
06830, Ankara, Turkey
kazimyuksel@aselsan.com.tr

[2] Department of Mechanical Engineering, Istanbul Technical University
34467, İstanbul, Turkey
{yukselka20, mugan}@itu.edu.tr

Abstract

In high-precision ground-based electo-optical object tracking, physical shock absorption and random vibration isolation devices play a critical role. These systems require three degrees of freedom translational shock absorbers in order to maintain exact orientation with the ground frame to achieve high precision angular position since any angular deviations that are unaccounted for can result in irreparable loss of sight of the object being tracked. Parallel manipulator-based absorption systems that have been currently in use consist of numerous hard to manufacture high precision backlash-free components and external springs that require protection against harsh environmental conditions and periodic maintenance. In this study, we focused on designing and optimizing maintenance-free flexure based compliant shock absorber mechanism with center of percussion optimized linkage that minimizes shock response. Linkage and flexure parameters were optimized in order to achieve minimal acceleration transmission while maintaining the orientation. A single degree of freedom system was designed and optimized. The Lagrangian method was used to derive equations of motion, and simulations were conducted based on these. This study put forth a fundamental framework for compliant translation shock absorber mechanism optimization and demonstrate in right configuration, with appropriately selected masses and optimized link parameters, that highly effective monolithic shock absorber and vibration isolation system can be achieved.

Keywords: Translational Shock Absorber, Vibration Isolator, Compliant Mechanism, Center of Percussion, Optimum Design.

ISSN:2623-3347
Peer-review under responsibility of the organizing committee of COMPDYN 2023.
doi: 10.7712/120123.10763.20614

1 INTRODUCTION

Environmentally challenging engineering applications require vibration isolation and shock absorption measures in order to protect sensitive equipment. In majority of these engineering applications, commercially available simplistic twisted steel wire rope isolators, metal mesh dampers, rubber viscoelastic dampers or bellow type air springs suffice the need. Wire rope isolators consists of looped twisted cables that dissipates energy by friction of the steel fibers [1]. Viscoelastic dampers, which are generally manufactured using high damping silicone, rubber or neoprene, dissipates energy using internal friction. These systems act as 6 degrees of freedom isolators. Lateral loading of such systems results in pitch and roll motion of the system. If the system is on a vehicle, turning motion results in yaw motion of the system relative to the base frame. Optical tracking devices require 3 degrees of freedom translational isolators in order to maintain exact orientation with ground frame to achieve high precision angular position since in 6 degrees of freedom passive systems, any angular deviations that are unaccounted for may result in irreparable loss of sight of the object being tracked [2]. In rotational stabilization systems, pointing vector of the system relative to ground frame is generally calculated using data from microelectromechanical systems (MEMS) based inertial measurement unit. Tuning fork based MEMS gyroscopes are susceptible to impulsive loading and vibrations which generates unwanted noise in readings [3]. These noises can result in failure of stabilization platform. Unwanted vibrations in MEMS device can be eliminated with isolators but use of 6 degrees of freedom system isolators mentioned above can result in rotation of coordinate system which is critical to the reading of velocities. Translational vibration isolators and shock absorbers can solve the stated problems.

In this study, single degree of freedom linkage system with revolute flexure bearings was designed and optimized. Lagrangian method was used to derive equations of motion of translational manipulator with link mass and inertia effects. Based on the equations of motion, Simulink model was built in order the optimize the shock response of the system. Screw theory based numerical modal analysis method [4] was used to iteratively optimize the link and flexure parameters. Mechanism design and equation of motion derivation of the mechanism are given in Section 2. Simulation results for the initial and optimized structure are given Section 3.

2 MECHANISM DESING AND EQUATION OF MOTION

A single degree of freedom shock absorber mechanism with symmetric linkages was designed. The mechanism consists of rigid links and flexure joints acting as revolute joints with torsional springs. A similar mechanism layout without flexures was used by Zeng et al. [5] that investigated the quasi-zeros stiffness effect as a part of vibration isolation method where they neglected the link masses and inertias. Quasi-zero stiffness effects are out of scope of this study where main target is optimization of link masses in order to achieve minimal acceleration transmission in payload mass.

2.1 Mechanism design and optimization parameters

Layout of the single degree of freedom mechanism with symmetric linkage and parameters are shown in Figure 1. Here, m_1 and m_2 are the link masses. m_p is the payload mass. $I_1$and I_2 are the link inertias. L is the link length. $L_{cm,1}$ and $L_{cm,2}$ are the center of mass distance from pivot points. y_b is the base excitation and the y_p is the payload displacement. θ_0 is the initial configuration angle of the system and θ is the deviation from initial angle. Joint torsional stiffness and viscous damping parameters are denoted by K_θ and B_θ, respectively. The same joint parameters were used for all three joints. Initial angle θ_0 was selected as $45°$.

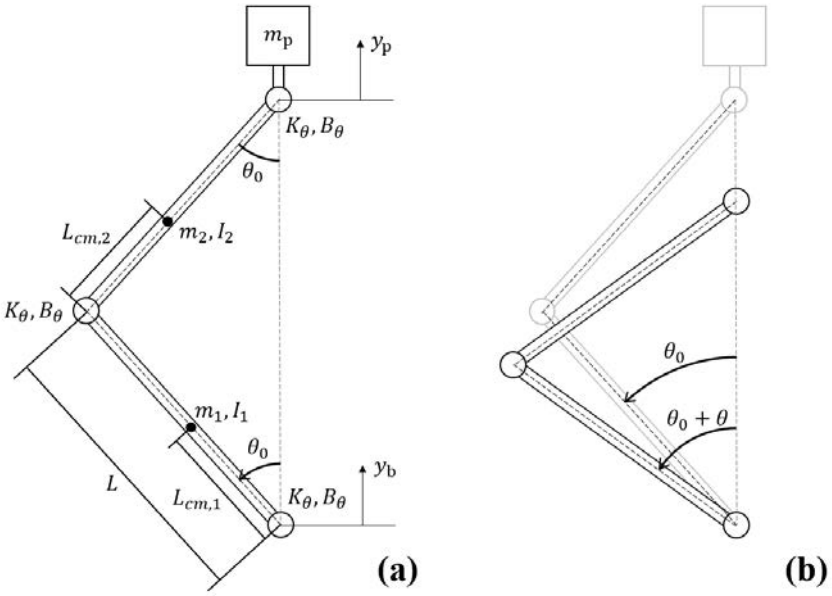

Figure 1: Designed 1 DOF Mechanism: mechanism parameters (a) and angle parameters (b).

The mechanism layout given in the Figure 1 does not constrain the motion of the payload to single degree of freedom in three-dimensional space. The mechanism is capable of motion in three degrees of freedom. In order to fully constraint the mechanism in unwanted motion, axisymmetric mechanism with at least three planar mechanism is required. Initial axisymmetric solid model with three planer linkages prior to optimization is given in Figure 2 below. Revolute joint selection criteria and calculations are given in Section 2.4.

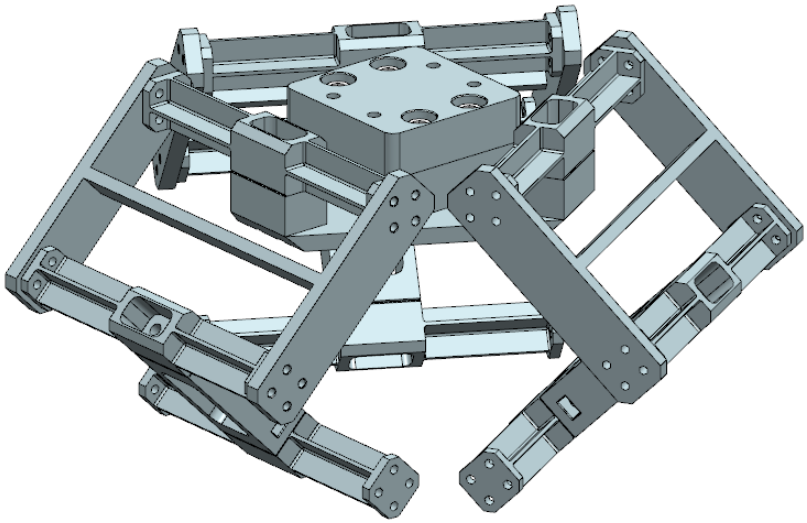

Figure 2: Designed 1 DOF Mechanism: mechanism parameters (a) and angle parameters (b).

2.2 System energy and equation of motion

In order to simulate the response of the system with base excitation, equation of motion of the system was required. The mechanism that was outlined in the Section 2.1 is an axisymmetric system. Therefore, modelling of the entire system was not required. One third of the system given in Figure 1 was sufficient to model the system. The parameters that were defined in

Section 2.1 was used in modelling of the system. Equation of motion of the mechanism was derived using Lagrange's energy equation which is expressed as:

$$\frac{d}{dt}\left(\frac{\partial KE}{\partial \dot{q}_i}\right) - \frac{\partial KE}{\partial q_i} + \frac{\partial PE}{\partial q_i} + \frac{\partial DF}{\partial \dot{q}_i} = Q_i \tag{1}$$

where KE, PE are respectively kinetic and potential energies, DF is the dissipative function, q_i is the generalized coordinate number i and Q_i is the generalized force acting on the generalized coordinate number i. Since it is a single degree of freedom passive system, generalized force can be assumed zero. The energy equations of system are evaluated with θ as the generalized coordinate.

Kinetic energy of the system is evaluated as:

$$\begin{aligned} KE \;=\; & \left[\frac{m_1}{2} + \frac{m_2}{2} + \frac{m_p}{2}\right]\dot{y}_b{}^2 \\ & + \left[\frac{I_1}{2} + \frac{I_2}{2} + \frac{m_1 {L_{cm,1}}^2}{2} + \frac{m_1\left({L_{cm,1}}^2 + L^2\right)}{2} - m_2 L L_{cm,2}\right. \\ & \left. + \left(2m_2 L L_{cm,2} + 2m_p L^2\right)\sin^2(\theta_0+\theta)\right]\dot{\theta}^2 \\ & + \left[\left(-m_1 L_{cm,1} - m_2\left(L + L_{cm,2}\right) - 2m_p L\right)\sin(\theta_0+\theta)\right]\dot{y}_b\dot{\theta} \end{aligned} \tag{2}$$

Potential energy of the system is evaluated as:

$$PE \;= \frac{1}{2}K_\theta\theta^2 + \frac{1}{2}K_\theta(2\theta)^2 + \frac{1}{2}K_\theta\theta^2 = 3K_\theta\theta^2 \tag{3}$$

Dissipative function of the system is evaluated as:

$$DF \;= \frac{1}{2}B_\theta\dot{\theta}^2 + \frac{1}{2}B_\theta\left(2\dot{\theta}\right)^2 + \frac{1}{2}B_\theta\dot{\theta}^2 = 3B_\theta\dot{\theta}^2 \tag{4}$$

Generalized force is evaluated as:

$$Q_1 \;= -2LF_{\mathrm{y}}\sin(\theta_0+\theta) \tag{5}$$

By using eq. (1), equation of motion of the designed system was evaluated as:

$$\left[I_{\mathrm{eq}}(\theta)\right]\ddot{\theta} + \left[N_{\mathrm{eq}}(\theta)\right]\dot{\theta}^2 + \left[B_{\mathrm{eq}}\right]\dot{\theta} + \left[K_{\mathrm{eq}}\right]\theta = \left[M_{\mathrm{b}}(\theta)\right]\ddot{y}_{\mathrm{b}} \tag{6}$$

where,

$$\begin{gathered} I_{\mathrm{eq}}(\theta) = I_1 + I_2 + m_1{L_{cm,1}}^2 + m_1\left({L_{cm,1}}^2 + L^2\right) - 2m_2 L L_{cm,2} \\ + \left(4m_2 L L_{cm,2} + 4m_p L^2\right)\sin^2(\theta_0+\theta) \\ N_{\mathrm{eq}}(\theta) = \left(4m_2 L L_{cm,2} + 4m_p L^2\right)\sin(\theta_0+\theta)\cos(\theta_0+\theta) \\ B_{\mathrm{eq}} = 6B_\theta \\ K_{\mathrm{eq}} = 6K_\theta \\ M_{\mathrm{b}}(\theta) = \left(m_1 L_{cm,1} + m_2\left(L + L_{cm,2}\right) + 2m_p L\right)\sin(\theta_0+\theta) \end{gathered} \tag{7}$$

Equation (6) gives the relationship between base excitation acceleration and link angle. Payload's position and acceleration was calculated using the trigonometric relationship in the symmetric linkage. Payload position can be calculated as $y_p = y_b + 2L\cos(\theta_0 + \theta)$.

2.3 System transfer function and center of percussion

In a single rigid body system with a finite mass and inertia, any impulsive load on the body will result in translation and rotation of the body in global frame, which means the motion of the system can be converted into rotation around an instantaneous rotation center. For rigid body that is connected to a pivot, if the instantaneous rotation center for the applied load coincides with the pivot, point where the impulsive force is applied is called center of percussion. At the instance of impulsive force application, pivot point will experience zero reaction force [6]. Since the instantaneous rotation center depend on center of mass, mass and inertia of the rigid body; center of percussion point can be optimized. This concept of zero reaction force by center of percussion optimization was used by Atik et al.[7] to design an optimal simple pendulum wishbone suspension system with minimal transmissibility to increase ride comfort. But in a compound linkage mechanism, center of percussion optimization of each link on its own does not guarantee the system's optimization. Garoi et al.[8] showed that in a compound link mechanism, system response tends to approach a finite value as frequency increases. This asymptotic value can be calculated using the transfer function of the compound system. In order to calculate the linear system transfer function, equation of motion of the system given in eq. (6) can be linearized by assuming $\dot{\theta}^2$ is negligible. Linear system's payload displacement to unit base excitation transfer function is evaluated as:

$$H(s) = \frac{Y_p(s)}{Y_b(s)} = \frac{\left(I_{\text{eq}}(\theta_0) - A(\theta_0)\right)s^2 + B_{\text{eq}}s + K_{\text{eq}}}{I_{\text{eq}}(\theta_0)s^2 + B_{\text{eq}}s + K_{\text{eq}}} \tag{8}$$

where $A(\theta_0)$ is,

$$A(\theta_0) = \left(2m_1 L L_{cm,1} + 2m_2 L\left(L + L_{cm,2}\right) + 4m_p L^2\right)\sin^2(\theta_0)$$

As it can be seen in the eq. (8), at high frequencies, system response asymptotically approaches to $\left(I_{\text{eq}} - A\right)/I_{\text{eq}}$ term. In order to minimize the response of the system with a decay at high frequencies, order of the numerator has to be reduced. Therefore, center of percussion criteria of the designed system expressed as:

$$I_{\text{eq}}(\theta) - A(\theta) = 0 \tag{9}$$

By applying an initial angle of 45°, the equation is reduced to:

$$\left(I_1 + m_1 L_{cm,1}\left(L_{cm,1} - L\right)\right) + \left(I_2 + m_2 L_{cm,2}\left(L_{cm,2} - L\right)\right) = 0 \tag{10}$$

which is the mechanism's percussion center condition with given initial angle condition. The terms in the equation corresponds to the percussion center condition of a single rigid body. Designed mechanism's center of percussion can be optimized either by optimizing each link on its own or by optimizing entire mechanism. It is important to state that 45° initial angle is a

special case of the mechanism where one can optimize the linkages individually because the links are perpendicular. For any other initial angle, optimizing each link on its own will not result in an optimized mechanism.

2.4 Flexure joints and stiffness calculation

Designed link mechanism uses revolute joints with torsional springs. Compliant counterpart of this joint is revolute flexure joints. Wide variety of revolute flexure joints exist in literature [9].Two commonly used joint types in industry are butterfly flexure and cross axis blade flexure joints which are shown in Figure 3. Both flexures are capable of large motion range. Cross axis blade flexure does a rolling motion instead of pure rotation. Therefore, a parasitic displacement is introduced to the mechanism. Off-axis stiffness of the both flexures degrade drastically as the joint rotates. In order for the designed mechanism to perform as single degree of freedom translational system, revolute flexure joint has to have near zero motion at axes other than designed revolute axis.

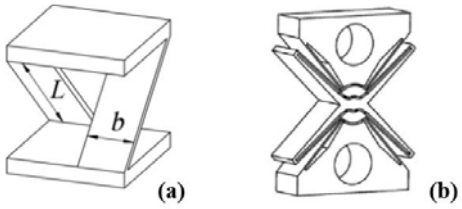

Figure 3: Revolute Flexure Joints. Cross Axis (a) and Butterfly (b).

Trease et al. [10] proposed a compact revolute joint capable of large deflection with cruciform cross section. Due to symmetry of the joint, it has pure rotation capability with zero axis drift in entire motion range while still maintaining large off-axis stiffness. Due to compactness and superior performance as revolute joint, cruciform cross section joint was selected to be used in the system. Layout and dimensional parameters of the joint given in Figure 4 below.

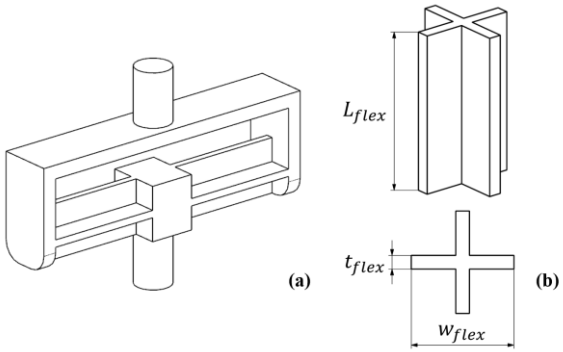

Figure 4: Cruciform Flexure Joint. Layout (a) and dimensional properties (b).

Proposed joint has two symmetric flexure elements with equal torsional stiffness Torsional stiffness of the single flexure joint with unconstrained boundaries is calculated with:

$$K_\theta = \frac{GJ}{L_{flex}} \tag{11}$$

where G is the shear modulus of the material, L_{flex} is the length of the flexure and J is the torsion constant of the cross section instead of polar inertia since the cross section is non-circular. Torsion constant for the cruciform cross-section can be approximated as [11]:

$$J = \left(\frac{w_{flex}}{\mathrm{t}_{flex}} - 0.373\right)\frac{2{t_{\mathrm{flex}}}^4}{3} \tag{12}$$

where w_{flex} is the width and t_{flex} is the thickness of the flexure. When the analytical stiffness calculated with eq.(10) and stiffness derived from finite element method (FEM) model compared, analytical model under estimated the stiffness. Since proposed revolute joint has non-circular cross section with fixed-clamped boundary conditions, end planes of the flexure cannot deform freely, restraint warping takes place which increases the stiffness of the flexure. Torsional stiffness of the flexure joint with constrained ends with warping effect is calculated with [12]:

$$K_\theta = \left(\frac{\beta L_{flex}}{\beta L_{flex} - 2\tanh\left(\frac{\beta L_{flex}}{2}\right)}\right)\frac{GJ}{L_{flex}} \tag{13}$$

where $\beta = \sqrt{GJ/EC_w}$. E is the Young's Modulus, G is the shear modulus and C_w is the warping constant of the cross-section. The parameter β is both dimensional and material property. For thin-walled closed sections, warping is usually small which is generally neglected [13]. But as the $L_{\mathrm{flex}}/w_{\mathrm{flex}}$ ratio of flexure link decreases, dominance of warping effects increases compared to torsion. Since warping constant of closed sections are generally neglected, analytical formulation of warping constant for cruciform cross-section could not be found in literature survey, therefore 2D finite element method (FEM) is used to calculate section parameters for a wide variety of dimensional parameters. Curve fitting is applied on 2D FEM data. Dimensional constant for the warping modification can be approximated as:

$$\sqrt{\frac{J}{C_w}} = \frac{1}{w_{flex}}\left(36.3\left(\frac{w_{flex}}{\mathrm{t}_{flex}}\right)^{-2.454} + 6.931\right) \tag{14}$$

Aluminum flexure joint was modelled in ANSYS with Young's Modulus of 71GPa and shear modulus of 26.692GPa. Torsional stiffness values of the revolute flexure joint proposed by Trease et al. [10] is compared with warping modified torsional stiffness and FEM results. Comparison of results is given in Table 1. As the $L_{\mathrm{flex}}/w_{\mathrm{flex}}$ ratio of flexure increases, warping effects become negligible. But becomes dominant as the $L_{\mathrm{flex}}/w_{\mathrm{flex}}$ ratio decreases. For compact flexure joints, torsional stiffness formulation alone can result in wrong modal frequencies since stiffness value can be lower.

L (mm)	w (mm)	t (mm)	FEM (Nm/rad)	Warping Modified Stiffness (Nm/rad)	Conventional Torsional Stiffness (Nm/rad)
64	32	1	11.613	11.494	8.794
64	32	2	90.982	90.737	69.519
64	32	4	686.847	703.175	542.874
640	32	1	0.894	0.901	0.879
640	32	2	7.022	7.118	6.952
640	32	4	53.650	55.554	54.287

Table 1: Torsional stiffness comparison of cruciform cross section for different dimensional parameters.

3 ANALYSIS AND OPTIMIZATION

The parametric model of the axisymmetric mechanism given in Figure 2 was built for optimization. For optimization case study, design choices, constants, optimization parameters are given as bullet points below:

- Shock isolator was designed with 2.3kg payload.
- 5Hz natural frequency was set as the optimization target.
- As shock input, 20g 11ms sawtooth profile was applied as base excitation.
- Link length L, was bounded between 60mm and 80mm with 1mm increments.
- Flexure length L_{flex}, was set as constant at 60mm.
- Flexure width w_{flex} was bounded between 24mm and 40mm with 1mm increments.
- Flexure thickness t_{flex} was bounded between 1.2mm and 3.6mm with 0.4mm increments due to 3D printer's capability of layer height increments.
- 3D print material PETG was selected as flexure material with Young's modulus of 1.6GPa, shear modulus of 579.7MPa and density of 1270 kg/m^3.
- 3D print material PLA was selected as link and payload base plate material with density of 1230 kg/m^3.
- Linkage was assumed as rigid.
- In order to optimize the percussion center of the mechanism according to eq.(10), only Link #1's center of mass was optimized with counterweights that were added to end points of Link #1.
- Torsional stiffness of the flexures are assumed to be linear.

The mechanism is parametrically designed in MATLAB algorithm that is based on the screw theory based meshless modal analysis method developed by Hopkins et al. for flexure analysis [4]. Payload mass is applied to the system as point mass. Optimization algorithm used analytical model of the mechanism to match the system natural frequency to optimization target using mass and inertia parameters generated by MATLAB algorithm. After frequency optimization, algorithm used brute force calculate counterweight mass to maintain center of percussion criteria given in eq. (9). The addition of counterweight changes the equivalent mass of the system which in return changes the natural frequency of the system. Therefore, frequency matching

and brute force center of percussion optimization steps repeated until parameters converged. Optimized structure with added counterweight is given in Figure 5 below. The parameters of the optimized structure are given in Table 2.

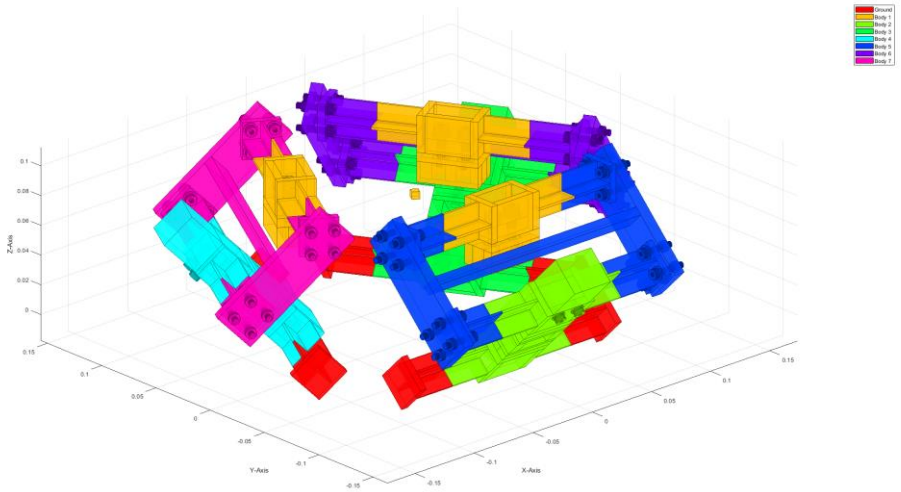

Figure 5: Parametrically designed and optimized 1 DOF mechanism with counterweight added to Link #1.

Optimization parameter	Parameters after optimization
L	65 mm
$L_{cm,1}$	44.1 mm
$L_{cm,2}$	32.5 mm
m_1	173.4 g
m_2	165.9 g
I_1	181.3 $kgmm^2$
I_2	153.8 $kgmm^2$
L_{flex}	60 mm
w_{flex}	25 mm
t_{flex}	1.6 mm
Natural Frequency	5.06 Hz

Table 2: Mechanism parameters after optimization.

In order to compare the response of the system prior to optimization and after, bode plots of the payload displacement to unit base excitation transfer function are given in Figure 6 below, in which initial system, optimized system and system with excessive counterweight which eight times the mass of the optimized counterweight, are compared. As it can be seen in the plots, response of the initial system converges to constant value at high frequencies whereas center of percussion optimized system has decayed.

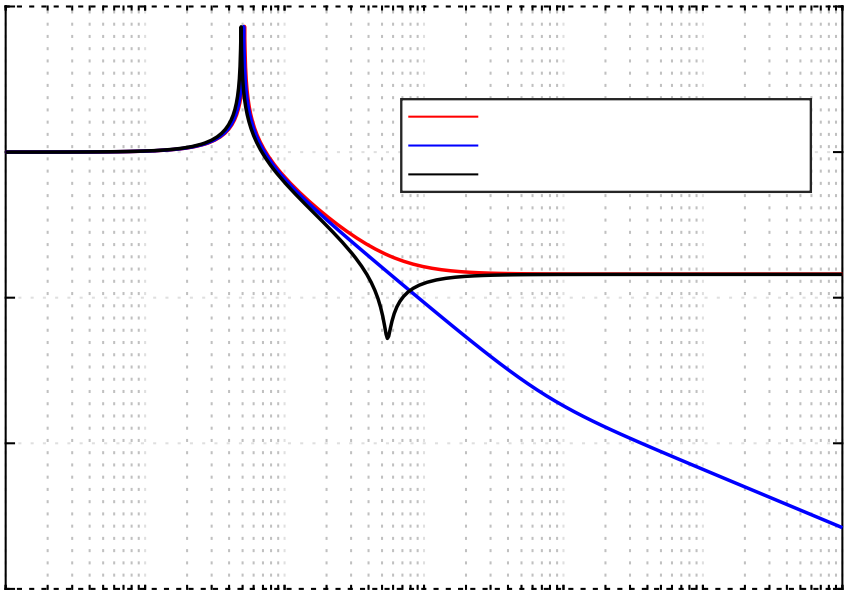

Figure 6: Comparison of the system response for different configurations.

In order to compare the shock response of the systems shown in Figure 6, Simulink model of system was built using the equation of motion. Layout of the Simulink model can be seen in Figure 7.

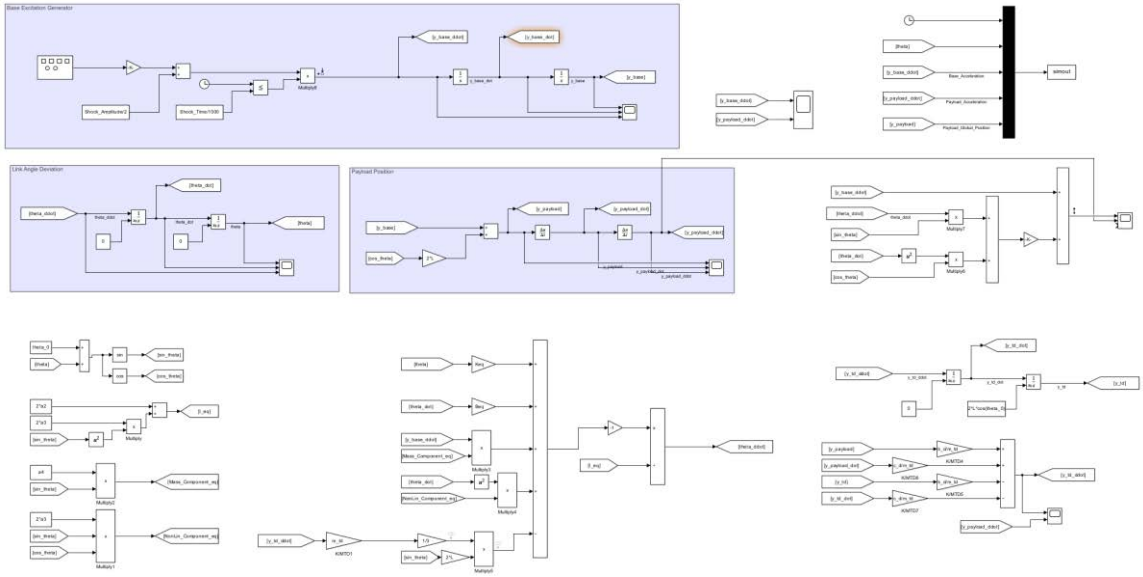

Figure 7: Layout of the Simulink model.

The shock response of the system with different initial condition are given below in Figure 8, Figure 9 and Figure 10. Shock duration comparison with different initial conditions is given in Figure 11.

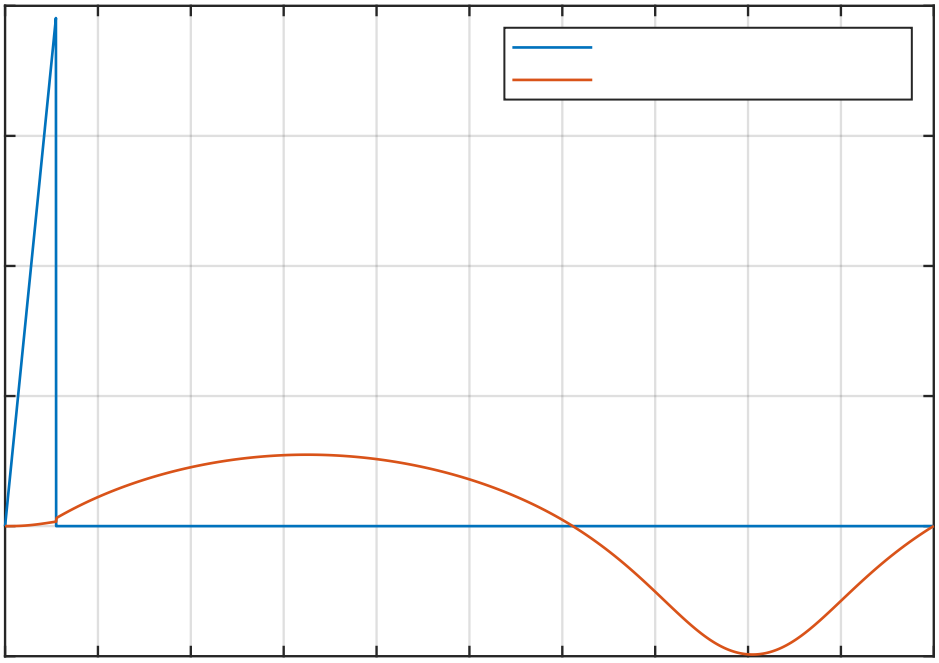

Figure 8: Center of percussion optimized system shock response.

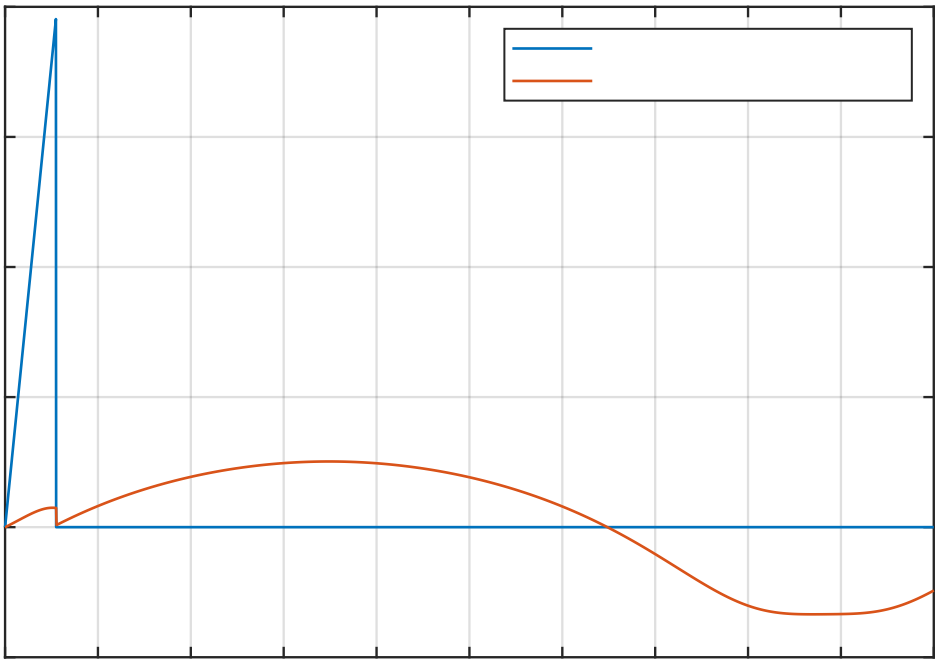

Figure 9: Shock response of the unoptimized system with excessive counterweight.

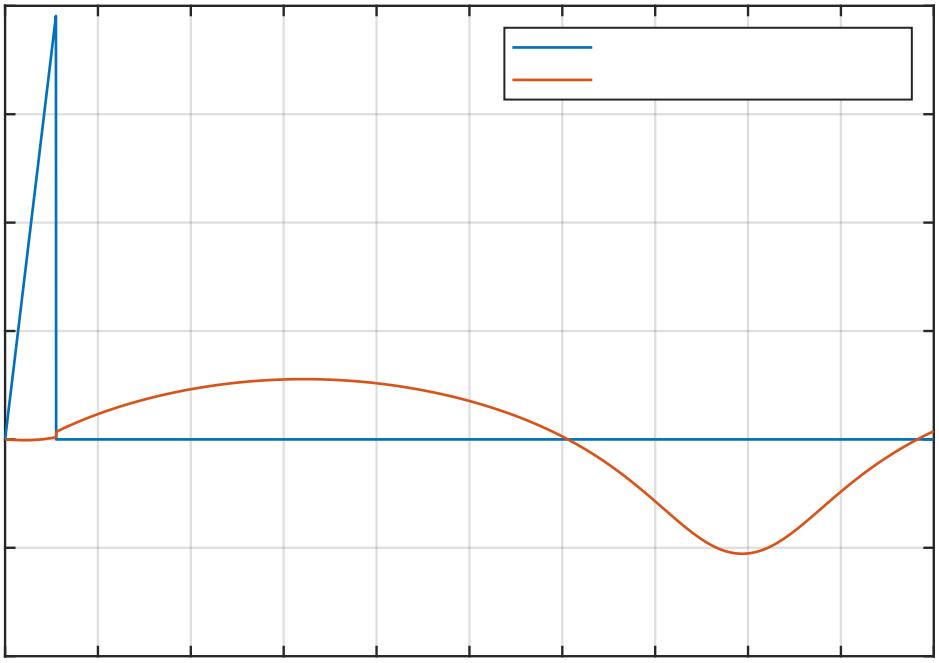

Figure 10: Shock response of the initial system prior to optimization.

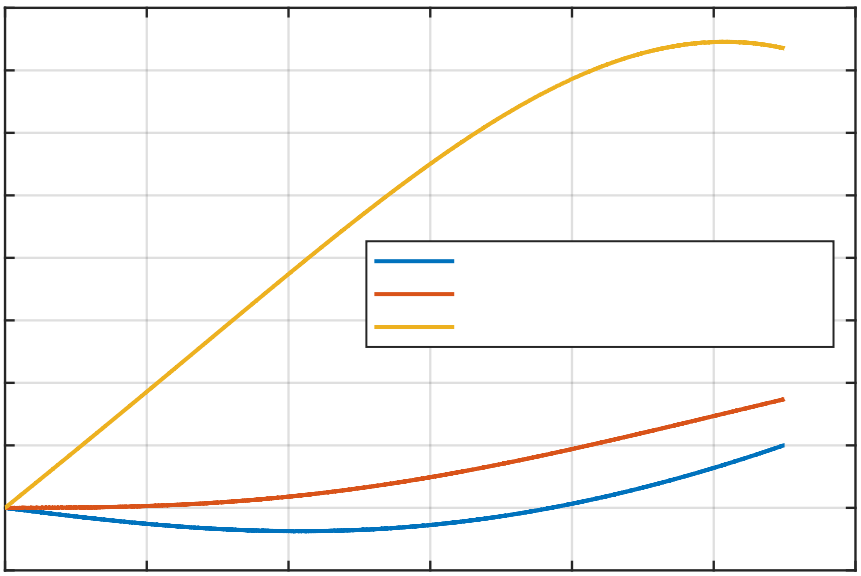

Figure 11: Shock response of all systems at the duration of the shock input.

As it can be seen in Figure 11, center of percussion optimized system has the least jerk, rate of change of acceleration, at the beginning of the shock. Initial system has the least peak acceleration. In the system with excessive counterweight, due to high inertia, links resists to rotation. Therefore, transmitting higher portion the of the shock to the payload.

Since the deformable linkage was out of scope of this study, one can say that initial system without the center of percussion optimization performed better at sawtooth shock response since peak acceleration was lower. But in deformable system with finite step jerk at the instance of shock application will result in high frequency residual vibrations in the payload which may be unwanted due to payload specifications. The responses given in Figure 11 is the result of 20g, 11ms sawtooth shock profile. If the amplitude, duration or the profile is changed, response characteristics change for unoptimized structures. But with center of percussion of the mechanism, minimum jerk condition holds.

4 CONCLUSIONS

The present work studied optimization of the compound link mechanism translational shock absorber and outlined a basic iterative optimization frame work for the given mechanism. This study showed that in a mechanism-based isolation structure, response of the structure can be further improved by merely adding a counterweight to the link to shift the link's center of mass to obtain mechanism's center of percussion. Center of percussion optimization of the mechanism at the initial angle will result in instantaneous zero acceleration of the payload but this does not mean the minimum response at entire shock duration. If system's deformed angle is known at the end of the shock duration, the system can be further optimized by maintaining an initial angle but shifting the optimization angle to the mean angle at shock duration. As the angle of the system deviates from the angle that center of percussion was optimized, effect of the optimization degrades. Therefore, by further optimizing the center of percussion angle, system can benefit optimally from the effect at entire shock duration. If the minimum peak acceleration is required, system can be optimized with the mean deformation angle. If the reduction of high frequency component is required, system can be optimized with initial angle.

In our future work, we will further investigate center of percussion effects in a 2 and 3 degrees of freedom system by optimizing structure to have minimal shock response independent of the direction of the applied load. Compliant tuned mass damper will be added to dampen out the residual harmonic oscillation after the shock input. Non-linear torsional stiffness effect caused by local elongation of the flexure will be modelled and used in optimization algorithm.

5 ACKNOWLEDGEMENTS

This study was conducted as a part currently ongoing Master's Thesis that is pursued at Istanbul Technical University as a part of Solid Mechanics Graduate Program with the cooperation of ASELSAN Academy. This study was funded by ASELSAN A.Ş.

REFERENCES

[1] K. Qi, L. Dai, S. Wang, Y. Yang, C. Fang and C. Lin, Design Methodology of a Passive Vibration Isolation System for an Optical System with Sensitive Line-of-Sight, *Photonic Sensors*, **11(4)**, 435-447, 2021.

[2] P. Balaji, M. Rahman, L. Moussa and H. Lau, Wire Rope Isolators for Vibration Isolation of Equipment and Structures - A Review, *IOP Conference Series: Materials Science and Engineering*, **78**, 2015.

[3] W. Y. Sang, L. Sangwoo and N. Khalil, Vibration-Induced Errors in MEMS Tuning Fork Gyroscopes, *Sensors and Actuators A: Physical*, **180**, 32-44, 2012.

[4] J. B. Hopkins, K. J. Lange and C. M. Spadaccini, Designing Microstructural Architectures with Thermally Actuated Properties Using Freedom, Actuation, and Constraint Topologies, *ASME Journal of Mechanical Design*, **135(6)**, 2013.

[5] R. Zeng, G. Wen, J. Zhou and G. Zhao, Limb-Ispired Bionic Quasi-Zero Stiffness Vibration Isolator, *Acta Mechanica Sinica*, **37**, 1152-1167, 2021.

[6] D. T. Greenwood, *Principles of Dynamics*, Prentice Hall, 1987.

[7] E. Atik, M. Karadeniz, A. Muğan, B. Keşli, A. Kanbolat, Optimum Design of Suspension Systems Under Kinematical Constraints, *SAE Technical Paper 2005-013608*, 2005.

[8] F. Garoi, J. Winterflood, L. Ju, J. Jacob and D. G. Blair, Passive Vibration Isolation Using a Roberts Linkage, *Review of Scientific Instruments*, **74**, 3487-3491, 2003.

[9] D. F. Machekposhti, N. Tolou, J L. Herder, A Review on Compliant Joints and Rigid-Body Constant Velocity Universal Joints Toward the Design of Compliant Homokinetic Couplings, *ASME Journal of Mechanical Design*, **137(3)**, 2015.

[10] B. P. Trease, Y. Moon, S. Kota, Design of Large-Displacement Compliant Joints, *ASME Journal of Mechanical Design*, **127(4)**, 788-798, 2015.

[11] S. T. Smith, *Flexures: Elements of Elastic Mechanisms – 1st Edition*, CRC Press, 2000.

[12] W. C. Young, R. G. Budynas, *Roark's Formula for Stress and Strain – 7th Edition*, McGraw-Hill, 2001.

[13] K. Rajagopalan, *Torsion of Thin Walled Structures*, Springer, 2022.